Figure S1, del Viso et al.

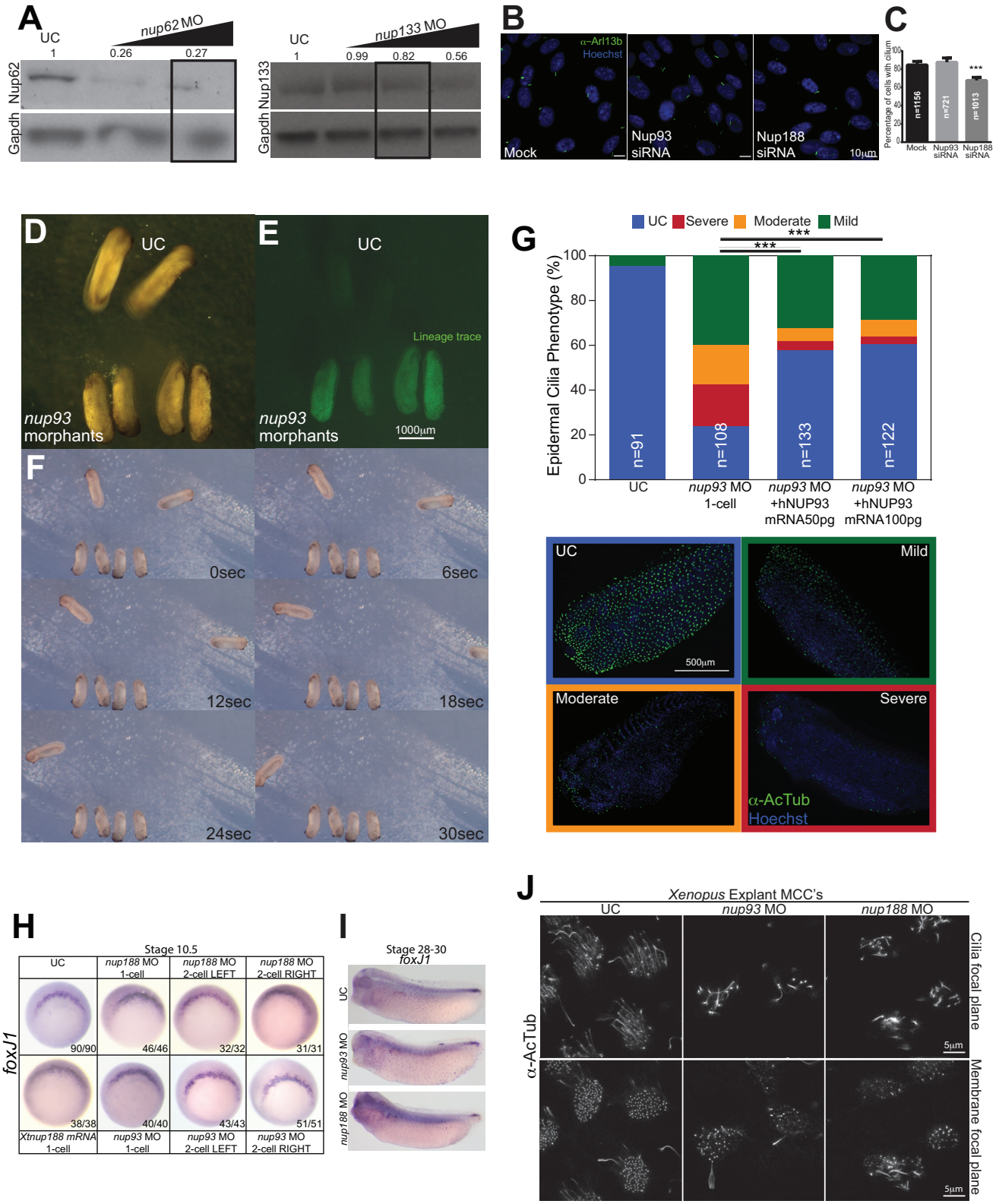

Figure S1 (related to Figures 1,2,3 and 4): Nup188 and Nup93 are required for cilia in mammalian cells and *Xenopus.*

(A) Nup62 and Nup133 protein levels after MO injection. Western blots of Nup62 and Nup133 in both uninjected controls (UCs) and embryos injected with *nup62* and *nup133* MOs (*nup62* MO doses: 5 and 10ng/embryo) (*nup133* MO doses: 2.5, 5 and 10ng/embryo). Numbers above each lane indicate the band intensity normalized to Gapdh (loading control). Boxed lanes indicate the dose used in epidermal cilia stain in Figure 3B.
(B) Nup188 is required for cilia in human RPE cells. Merged (green and blue channels) fluorescent images of human RPE cells induced to ciliate after knockdown of Nup188 or Nup93 using specific siRNAs or scrambled (mock) control. Cilia are stained with an Arl13b antibody (green) and DNA with Hoechst (blue). See also Figure 4F and 4J for degree of knockdown.
(C) Nup188 depletion in RPE cells leads to decreased ciliation. Plot of percentage of ciliated cells after knockdown of Nup188 or Nup93 using specific siRNAs in human RPE cells. n=total number of nuclei/cilia from 3 independent experiments. Chi-Square Test, *** $p<0.0005$.
(D-F) Loss of *nup93* affects gliding in *Xenopus* embryos.
(D) At stages 28-31, wildtype embryos glide along the surface of an agarose-coated dish due to the beating of multiciliated cells while *nup93* morphants do not. Brightfield images of 2 UCs (top) and 4 *nup93* morphant embryos (bottom).
(E) Same field as (D) but *nup93* morphants are identified by Alexa488 tracer dye (bottom 4 green morphants).
(F) Video frame captures of the same UC and morphant embryos in (D) and (E) gliding at indicated times. See also Movie S1.
(G) Nup93 is specifically required for epidermal cilia. Plot of the percentage of embryos with abnormal epidermal cilia assessed by anti-AcTub staining after injection at 1-cell stage with *nup93* MO (1 ng/embryo) or (to assess specificity) with *nup93* MO combined with human (h) NUP93 mRNA (50 or 100 pg/embryo). Bottom panel is a key (blue, green, orange, red) to our qualitative assessment of cilia shown as example fluorescent images of embryos (lateral views, dorsal at top) stained with anti-Actub (green) and Hoechst (blue). n=total number of nuclei/cilia from 3 independent experiments, Chi-Square Test, *** $p<0.0005$.
(H-I) Cilia loss in nup morphants is not due to changes in cilia cell type specification.
(H) *In situ* hybridizations images with a *foxj1*-specific probe of stage 10.5 embryos injected with the indicated MOs or with *Xtnup188* mRNA. Vegetal views of embryos with blastopore lip to the top are shown as representative examples of 2 independent experiments. Numbers indicate the number of embryos showing the same staining pattern.
(I) *In situ* hybridizations images with a *foxj1*-specific probe of stage 28-31 embryos injected with the indicated MOs. Left, lateral views of embryos with dorsal at the top are shown as representative examples of 3 independent experiments.
(J) Nup188 and Nup93 depletion affects multiciliated cells in *Xenopus* epidermis. Fluorescent images of epidermal animal caps derived from UC embryos or those injected with the indicated MOs; multiciliated cells (MCCs) labeled with anti-AcTub (green). Two z-sections (top and bottom panels) at the indicated focal planes are shown.

Figure S2, del Viso et al.

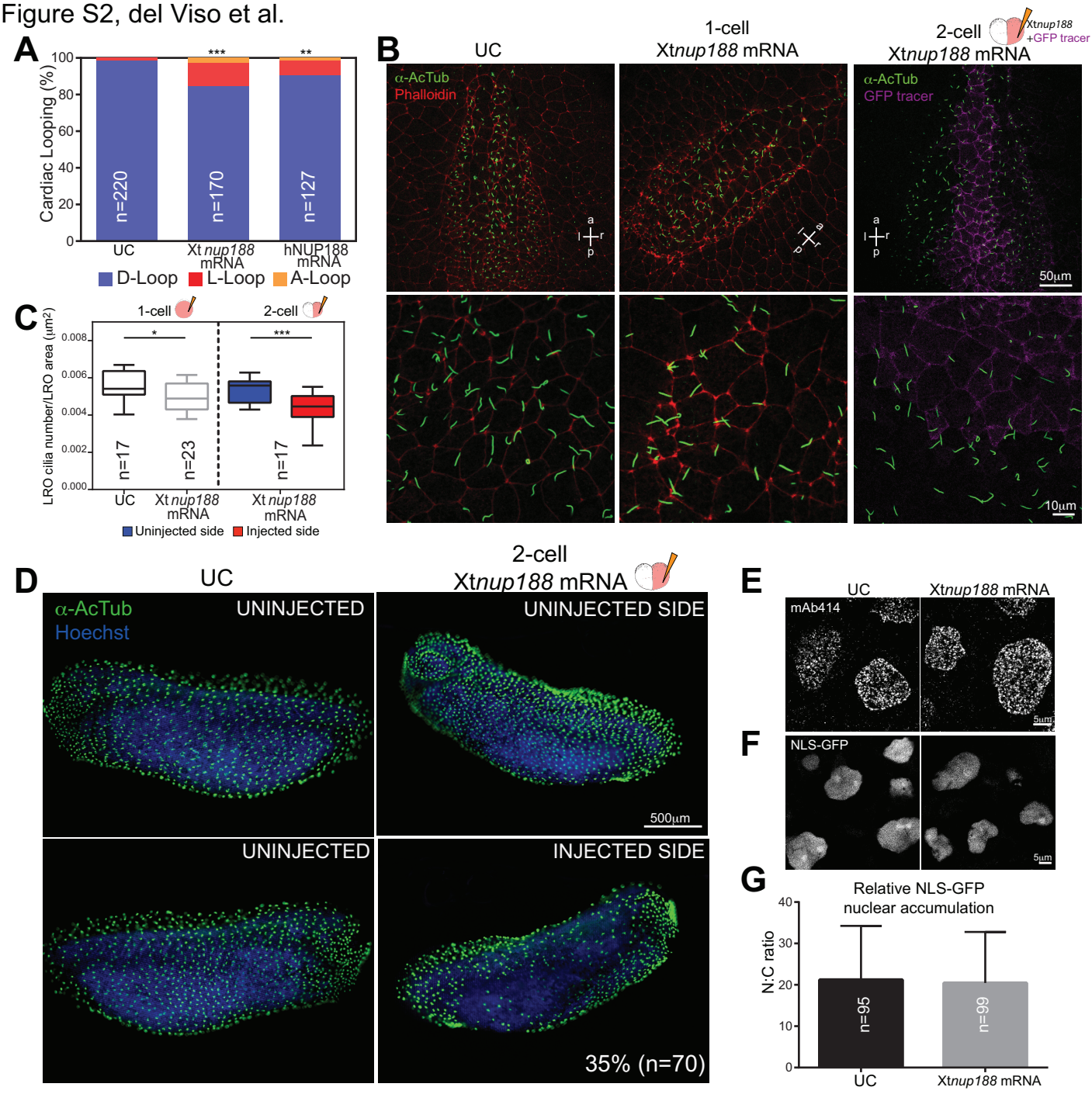

Figure S2 (related to Figures 1, 2 and 3): Nup188 overexpression specifically affects cardiac looping and cilia.

(A) Overexpression of Nup188 affects heart looping. To drive overexpression of Nup188, *Xenopus tropicalis (*Xt*) nup188* mRNA or human (h) NUP188 mRNA were injected at 1-cell stage. Plot shows the percentage of resulting embryos with cardiac looping defects. Chi-Square or Fisher's Exact Test, ***p<0.0005, **p<0.05. n=total number of embryos from 3 independent experiments.

(B) LROs from control embryos (UC) and embryos injected with the Xt*nup188* mRNA at the 1 or 2-cell stage. Primary cilia were stained with anti-AcTub (α-AcTub, green). Phalloidin was used to mark cell borders (red). Xt*nup188* mRNA was traced using an mRNA encoding for a GFP-tagged plasma membrane protein (magenta). p,a,l,r: posterior, anterior, left, right, respectively.

(C) Box plots show cilia number per LRO area (μm^2) of UC and embryos injected at the 1 or 2-cell stage with Xt*nup188* mRNA. The box depicts the 25th to 75th percentiles with the median marked as a horizontal line. The whiskers mark the data range from the smallest to the largest value. In embryos injected at the 2-cell stage, blue boxes are the uninjected side and red boxes the injected side. n=total number of embryos from 2 independent experiments, T-test, *** p<0.0005, * p<0.05.

(D) *Xenopus* embryos were injected with Xt*nup188* mRNA into 2-cell stage such that half the embryo receives the mRNA (See Figure 1A for a visual guide to these experiments). Fluorescence images are lateral views, with dorsal at the top, of both sides (uninjected and injected) of a single embryo with the cilia of the MCCs labeled with anti-AcTub (green). Nuclei stained with Hoechst (blue). The disruption of cilia on the injected side was found in 35% (n=70) of embryos from 2 independent experiments.

(E) Fluorescent images of NPCs stained with the mAb414 antibody in animal caps of UC and embryos injected with Xt*nup188* mRNA.

(F) Fluorescent images of embryos co-injected with mRNA encoding NLS-GFP and Xt*nup188* mRNA. Animal caps were dissected and allowed to develop MCCs before imaging.

(G) Embryos were co-injected with mRNA encoding NLS-GFP and Xt*nup188* mRNA. Graph shows the nuclear/cytoplasm (N:C) ratio of mean NLS-GFP fluorescence intensities and the SD. n=total number of nuclei from 3 independent experiments.

Figure S3, del Viso et al.

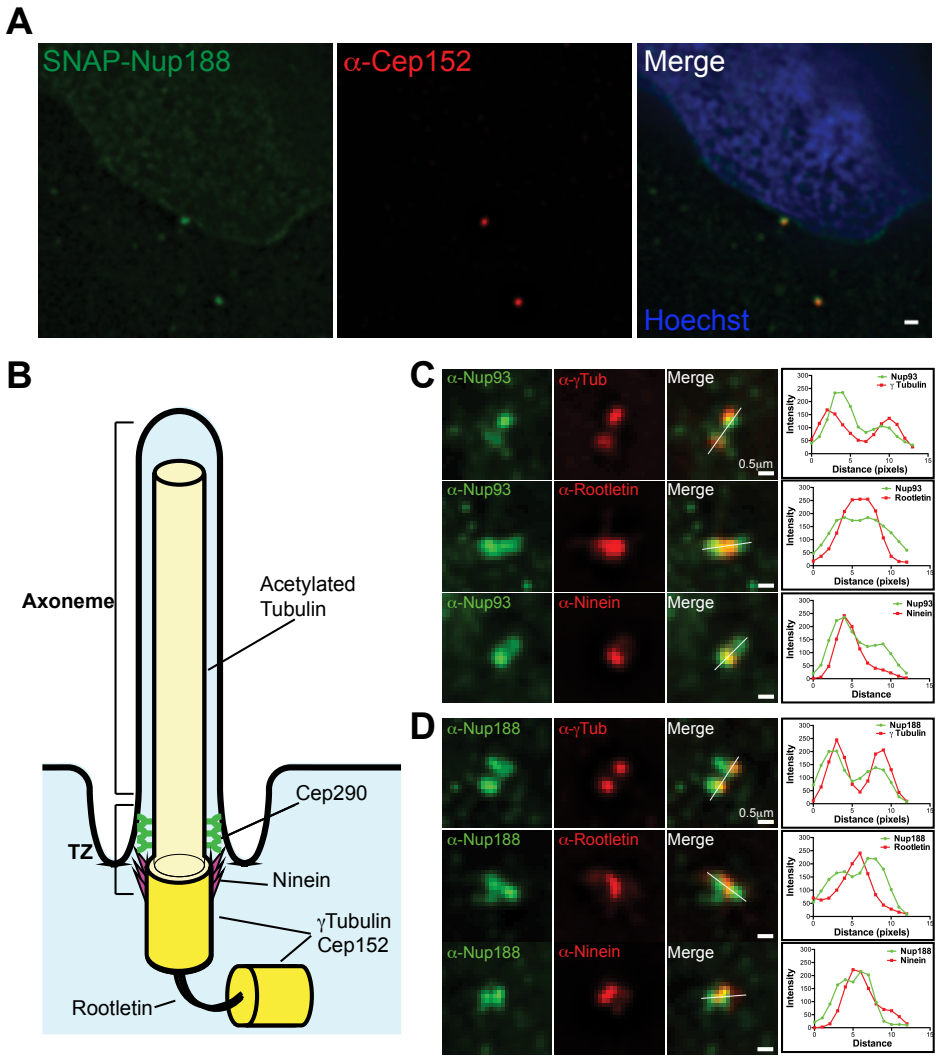

Figure S3 (related to Figure 4): Nup93/188 localize to the mother and daughter centriole.
(A) An overexpressed SNAP-Nup188 co-localizes with centrioles. Fluorescent micrographs of HeLa cells expressing SNAP-Nup188 detected with the oregon-green SNAP substrate. Centrioles were detected with an anti-Cep152 antibody (red) and DNA stained with Hoechst (blue) in merge panel.
(B) Schematic of the cilium. BB is basal body (mother centriole), DC is daughter centriole and TZ is transition zone.
(C) Nup93 localizes to the BB and DC. Deconvolved fluorescent micrographs of the bases of cilia in RPE cells immunostained with the indicated anti-Nup93 antibodies (green) and those that stain different components of the cilium base (red). Pixels under the white line in merged image were used to generate line profile plots in right panels.
(D) Nup188 localizes to the BB and DC. Deconvolved fluorescent micrographs of the bases of cilia in RPE cells immunostained with the indicated anti-Nup188 antibodies (green) and those that stain different components of the cilium base (red). Pixels under the white line in merged image were used to generate line profile plots in right panels.

Figure S4, del Viso et al.

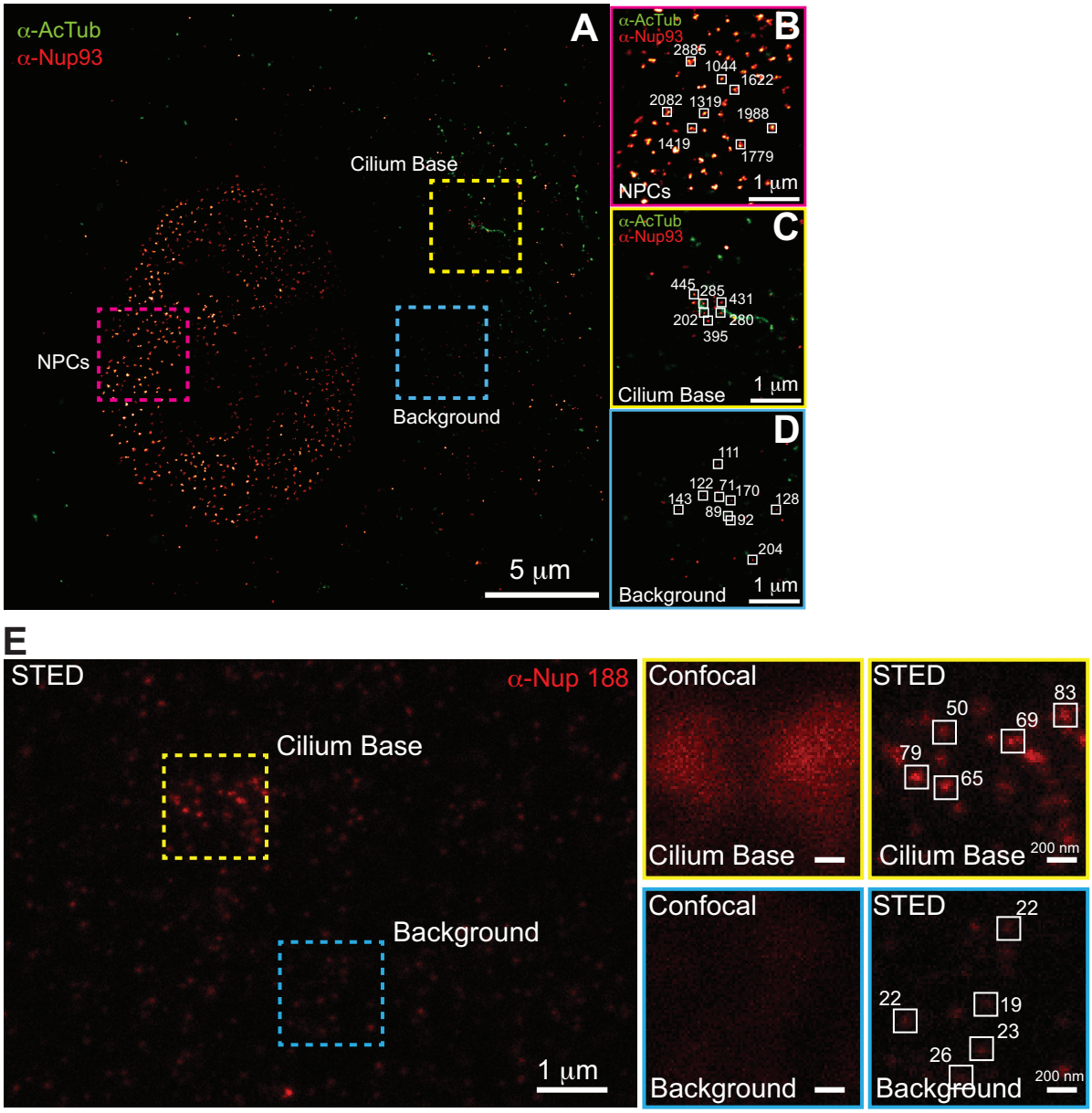

Figure S4 (related to Figure 5): Comparison of number of detections per cluster for both Nup93 and Nup188 in 2D-FPALM and fluorescence intensity in STED.
(A) Two-color 2D-FPALM image of cell labeled with anti-AcTub (green) and anti-Nup93 (red). Three boxed ROIs from the nuclear surface, the cilium base, and the cellular background are magnified in **B-D**.
(**B-D**) Magnification of the three ROIs shown in panel A showing number of localizations for a selected number of clusters (white boxes) in all three ROIs.
(E) STED images of immunolabeled anti-Nup188 clusters at the cilium base. ROIs are selected from both the cilium base and the cellular background to show the increased fluorescence intensity (in arbitrary units) of clusters at the basal body (far right panels, white boxes). Diffraction limited confocal images are also shown in middle panels.

Figure S5, del Viso et al.

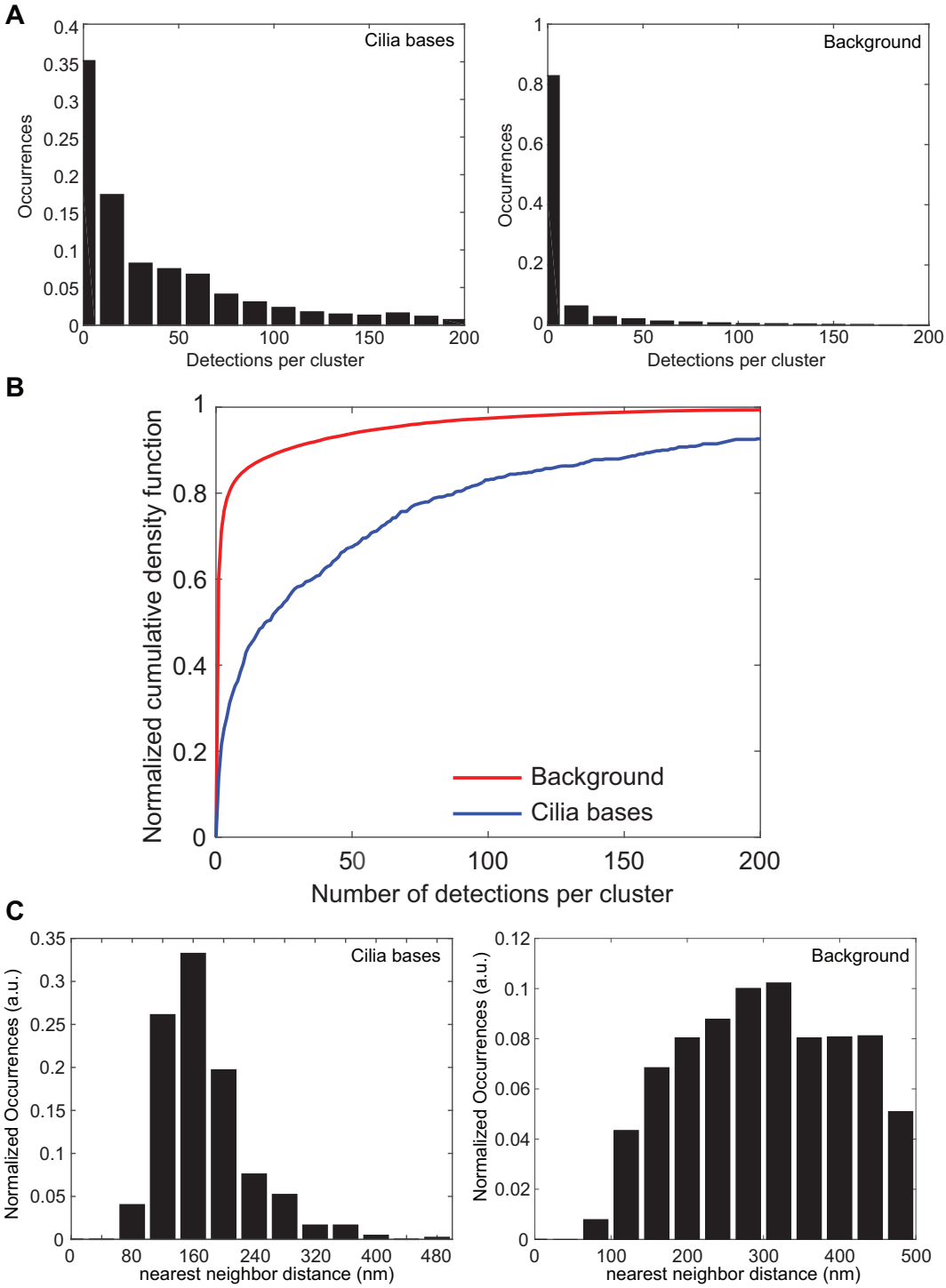

Figure S5 (related to Figure 6): Nup188 is found in multiple copies within evenly spaced clusters at the cilium base.

(**A**) The number of anti-Nup188 localizations (detections) per cluster from 10 W-4PiSMSN images of cilia bases (left) and corresponding randomly selected regions (right).

(**B**) Cumulative density distribution of data shown in A for better visualization of histograms.

(**C**) Nearest neighbor distance distribution between the cilia bases (left; reproduced from Figure 6B) and randomly selected locations from 17 images (right). a.u. is arbitrary units.

Figure S6, del Viso et al.

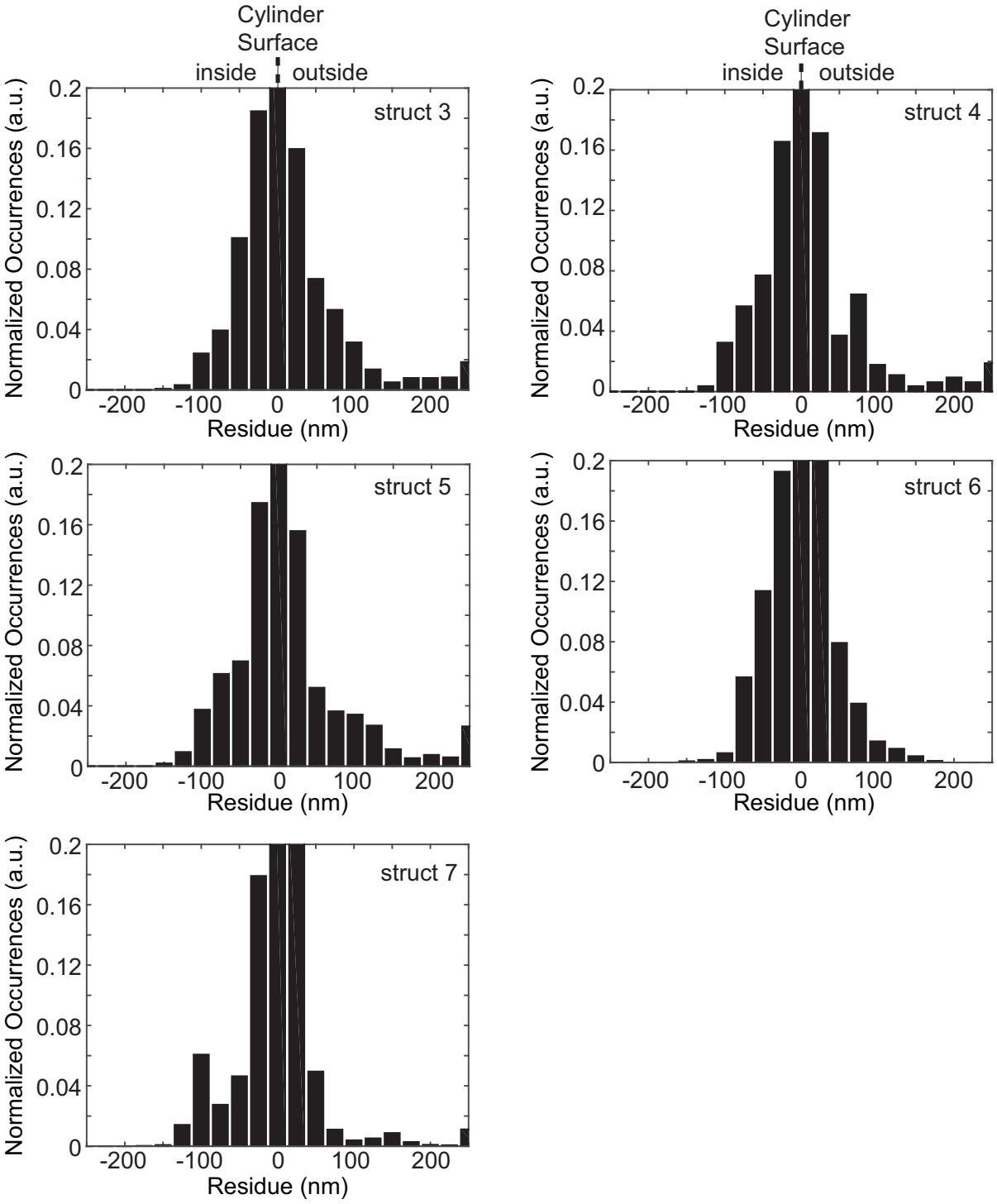

Figure S6 (related to Figure 6 and movie S3): Distribution of anti-Nup188 single molecule detections with reference to cylinder surface.
Distribution of the distances of single molecule detections of 5 cylinder-modeled Nup188 structures (see Movie S3) showing a compact distribution around the cylindrical surface. Negative values indicate the detections are within the cylinder and positive values are outside.

Supplemental Movie Legends:

Supplemental Movie S1 (related to Figure S1D): Knockdown of Nup93 alters gliding in *Xenopus* embryos. Two wildtype embryos (top) and four *nup93* morphants (bottom) are positioned on an agarose coated dish (stages 28-31). Wildtype embryos glide due to the beating of epidermal cilia. *nup93* morphants fail to glide (identity of morphants is confirmed by the co-injection of an Alexa488 dye, see Figure S1).

Supplemental Movie S2 (related to Figure 6): Nup188 surrounds the centrioles in evenly spaced clusters that organize into two barrel-like structures

Movie S3 (related to Figure 6): 3D movies of W-4PiSMSN data of multiple barrel structures with cylinder fits.

Supplemental Experimental Procedures

Frog husbandry

X. tropicalis were housed and cared for in our aquatics facility according to established protocols that were approved by Yale IACUC.

Microinjection of MOs and mRNA in *Xenopus* embryos

We induced ovulation and collected embryos by *in vitro* fertilization according to established protocols (del Viso and Khokha, 2012). Embryos were raised to appropriate stages in 1/9MR +gentamycin. Staging of *Xenopus* tadpoles was performed according to Nieuwkoop and Faber (Nieuwkoop and Faber, 1994). Antisense morpholino oligonucleotides (MO) or mRNAs were injected at either the one cell stage or into one cell of the two-cell embryo as previously described (Khokha et al., 2002). The following MOs were used: *nup62* ATG blocking (5-10ng/embryo 5' CACTCATAGTGGTCAATTCTGATCC), *nup93* ATG blocking (1-2 ng/embryo 5'TCCAAACCCTTCTCCATCCATTGTC), *nup133* ATG blocking (2.5,5,10 ng/embryo 5' CCGCTGTGTCGGGATAGTTTGAAAA), *nup188* ATG blocking (2,4,6 ng/embryo 5' CCATCTTCACGCCCCCTTCACGGCC). Alexa488 (Invitrogen), mini-ruby (Invitrogen), or mRNA encoding GFP (100 pg/embryo) were injected as tracers. We generated human *nup188* mRNA by cloning the ORF from IMAGE clone 100064128 (Open Biosystems, Dharmacon) into the pCSDest vector using Gateway recombination techniques (Invitrogen, Life technologies). We generated *X. tropicalis nup188* mRNA by cloning the ORF from IMAGE clone 7675066 (Open Biosystems, Dharmacon) into pCS108 using NotI and SalI. To generate human NUP93 mRNA, we obtained the HsCD00332518 clone from PlasmID at Harvard Medical School and after sequence verification, we corrected a base pair change (nt 1558, G to C) using site-directed mutagenesis (QuikChange II, Agilent Technologies) to restore coding for arginine at position 509, which is conserved in most vertebrate species and is the annotated sequence in the human genome. We generated *in vitro* capped mRNA using the SP6 mMessage machine kit (Ambion) following the manufacturer's instructions.

To test whether overexpression of Nup188 affected organ *situs*, we injected 100 pg/embryo of *X. tropicalis nup188* mRNA or human NUP188 mRNA at the 1 cell stage or in one cell of the 2-cell stage combined with 100 pg/embryo of an mRNA encoding a plasma membrane GFP as a tracer. To test the specificity of the MO, we rescued *nup188* morphants by injecting 2 ng/embryo of the *nup188* MO at the 1 cell stage, followed by 12 pg/embryo of human NUP188 mRNA into one cell at the 2 cell stage. Cardiac looping was scored 3 days post fertilization as described below. To rescue *nup93* morphants, we injected 1 ng/embryo of *nup93* MO yielding a range of phenotypes, which we qualitatively assessed as 'mild', 'moderate' and 'severe' and compared to embryos co-injected with human NUP93 mRNA (50 or 100 pg/embryo) at the 1 cell stage. For NPC function assays in animal caps, MOs were co-injected with 100 pg/embryo of NLS-GFP mRNA (plasmid p3E-IRES-nlsEGFPpA, a gift from the Chien lab (Kwan et al., 2007)).

Cardiac looping in *Xenopus*

Frog embryos at stage 45 were treated with benzocaine and ventrally scored for cardiac looping using a light dissection microscope as previously described (Boskovski et al., 2013). Loop direction is defined by the position of the outflow tract relative to the inflow of the heart: outflow to the right – D loop; outflow to the left – L loop; outflow midline – A loop (Figure 1C).

Whole mount *in situ* hybridization

We detected *Xenopus coco*, *foxj1* and *pitx2c* expression by generating Digoxigenin-labeled antisense probes using the T7 High Yield RNA Synthesis kit (NEB, E2040S) and DIG-dUTP (Roche). Clone numbers are the following: *coco*: TEgg007d24, *foxj1*: Tneu058M03, *pitx2c*:

TNeu083k20. Embryos were collected at the desired stages (*foxj1*: stages 10.5 and 28-31 and *pitx2c:* stages 28-31), fixed in MEMFA (1:1:8 10X MEMFA salts, 37% formaldehyde, distilled water)(10x MEMFA salts: 1 M MOPS, 20 mM EGTA, 10 mM $MgSO_4$) for 1-2 h at room temperature and dehydrated in 100% ethanol. LROs to study *coco* at post-flow stages were collected at stages 19-20, fixed in 4% PFA at room temperature for 1 h, dissected in MBSH (88 mM NaCl, 1 mM KCl, 0.41 mM $CaCl_2$, 10 mM HEPES, 0.33 mM $Ca(NO_3)_2$, 0.82 mM $MgSO_4$, 2.4 mM $NaHCO_3$) as previously described (Schweickert et al., 2007) and dehydrated into 100% ethanol. Whole mount *in-situ* hybridization was done as previously described (Khokha et al., 2002). Embryos were scored for *pitx2c* expression in the lateral plate mesoderm (Schweickert et al., 2000) (Figure 1E). LROs were scored for *coco* expression as previously described (Schweickert et al., 2010) (Figure 1G).

Gliding assays

Embryos were injected at the one cell stage with either 2 ng of *nup93* MO along with an Alexa488 tracer (Life Technologies). At stages 28-30, control and morphants embryos were placed in a Petri dish with 1% agarose, and muscle contractions were inhibited with benzocaine. Their movement was captured for 30 seconds using a Canon EOS 5d digital camera mounted on a Zeiss discovery V8 stereomicroscope. Brightfield and fluorescent pictures were taken using a Zeiss SteREO Lumar.V12 fluorescent microscope and an AxioCamHR3 digital camera in conjunction with ZEN 2012 (Blue Edition, version 1.1.2.0) software.

Animal caps

Animal Caps from stage 9 control and morphant embryos were dissected as described (Werner and Mitchell, 2013), using forceps instead of an eyebrow knife. Explants were attached to round coverslips pre-treated with fibronectin (Roche) as described (Werner and Mitchell, 2013) and allowed to develop overnight at 26^{o}C. Coverslips were placed in a 24-well plate and processed for immunofluorescence (IF).

Antibodies (Abs)

Ab Type	Antigen (dilution used)	Source
Primary	anti-*Xenopus laevis* Nup188 (1:1000)	W. Antonin(Theerthagiri et al., 2010)
	anti-*Xenopus laevis* Nup93 (1:2000 WB, 1:1000 IF)	W. Antonin(Franz et al., 2007)
	anti-human Nup188 (1:1000 WB, 1:500 IF)	A302-322A, Bethyl Laboratories
	anti-*Xenopus laevis* Nup133 (1:1000)	M. Dasso(Mishra et al., 2010)
	anti-human Nup62 (1:1000 WB, IF)	BD Transducton Laboratories
	anti-Nup358 (1:1000)	E. Coutavas, G. Blobel
	anti-TPR (1:1000)	E. Coutavas ,G. Blobel
	mAb414 (1:1000)	24609, Abcam
	anti-acetylated α-tubulin (AcTub)(1:1000)	T6793, Sigma
	anti-Arl13b (1:250)	75-287, UC Davis/NIH NeuroMab
	anti-γ-Tubulin (1:100)	T6557, Sigma
	anti-Rootletin (1:100)	sc67824, Santa Cruz
	anti-Ninein (1:1000)	sc50142, Santa Cruz
	anti-CEP290 (1:2000	ab85728, Abcam
	anti-GAPDH (1:5000, WB).	Ambion, AM4300
Secondary	Alexa Fluor (AF) 488 anti-mouse and anti-rabbit, AF594 anti-mouse, AF647: anti-	Life Technologies

	mouse, anti-rabbit and anti-goat (all used 1:500)	
	ATTO647N anti-mouse and anti-rabbit (1:1000)	Active Motif
	ATTO594 anti-mouse and anti-rabbit (1:1000)	Active Motif
	Cy3B NHS Ester was coupled to AffiniPure Goat Anti-Mouse or Anti-rabbit IgG (H+L) secondary antibodies via the manufacturer's specifications (1:200 IF).	GE Healthcare, PA63100 Jackson,115-005-003, 111-005-003
	anti-mouse or anti-rabbit HRP conjugated (1/10000, WB)	Jackson Immuno Research Laboratories, 715–035–150 (mouse) or 211–032–171 (rabbit)

Western blots

To isolate protein from *Xenopus* embryos, control or morphant embryos were collected and placed in 1x RIPA buffer (10 µl/embryo) (Cell Signaling, 20 mM Tris-HCl (pH 7.5), 150 mM NaCl, 1 mM Na_2EDTA, 1 mM EGTA, 1% NP-40, 1% sodium deoxycholate, 2.5 mM sodium pyrophosphate, 1 mM β-glycerophosphate, 1 mM Na_3VO_4, 1 µg/ml leupeptin) supplemented with protease inhibitors (Complete, Roche). For *nup93* and *nup188* morphants (Figure 1I), we collected stages 35-37 embryos for Western blots. For *nup62* and *nup133* morphants, we collected stages 25-29 embryos for Western blots (Figure S1A). Embryos were then crushed using a pestle and centrifuged at 12000 rpm for 10 min at 4°C, to separate protein from lipids and debris. Human RPE cells were lysed using the same RIPA buffer and spun down similarly at 4°C. We quantified protein concentration in supernatants using DC Protein Assay (Biorad). Western blotting was performed following standard protocols. Anti-GAPDH was used as loading control. For detection, we used the following secondary antibodies: anti-mouse or anti-rabbit HRP conjugated secondary and Western lightning Plus ECL (Perkin Elmer). Quantifications of changes in protein levels were calculated using Fiji/ImageJ software (Schindelin et al., 2012) by normalizing to GAPDH levels.

Cell culture and siRNA experiments

Human Tert-RPE1 (human telomerase-immortalised retinal pigmented epithelial; herein RPE) cells were maintained in DMEM/Ham's F12 supplemented with 10% fetal bovine serum (FBS) and antibiotics at 37ºC and 5% CO_2. Cells were grown to confluency and starved for 48 h to allow cilia growth before IF. For siRNA experiments, cells were transfected with siRNAs using Lipofectamine RNAiMAX transfection Reagent (Life Technologies) following the manufacturer's instructions. We purchased the following Stealth siRNAs from Life Technologies: siRNA Negative Control, Med GC, Cat. No.: 12935-300 (Mock), NUP93: HSS114514 and NUP188: HSS146447. For NUP93 siRNA, we used 1.5 µl of Lipofectamine+25 pmol of siRNAs per well, and for NUP188, we used 2.5 µl of lipofectamine+25 pmol of siRNA per well (24-well plate). Cells were incubated with siRNA mix overnight in media without serum (FBS). The next day cells were transferred to media supplemented with 10% FBS for 36 h and then were starved in media without serum for additional 48 h, before fixation.

Statistical analysis

All experiments were performed a minimum of two times and numbers stated in graphs are the composite of multiple experiments. Statistical significance of cardiac looping, *pitx2c* and *coco* abnormalities, as well as the *nup93* rescue experiment and the cilia reduction in RPE cells upon

Nup188 siRNA, was tested using Chi-squared or Fisher's Exact test. The significance of the amount of cilia in LROs was evaluated using paired (for injections at 2-cell stage) or unpaired, two-tailed student's t- tests (Figures 2 and S2C) using GraphPad Prism version 6.00, GraphPad Software, La Jolla California USA, www.graphpad.com. The statistical significance of the intensity reduction after siRNA depletion of NUP93 and NUP188 at the nuclei or base of cilia in RPE cells was tested using unpaired, two-tailed student's t- tests (non-parametric) using GraphPad (Figures 4E and 4I). In all Figures, statistical significance was defined as $p<0.05$. A single asterisk indicates $p<0.05$, while double and triple asterisks indicates $p<0.005$ and $p<0.0005$, respectively.

Immunostaining and SNAP labeling

All immunostaining procedures were performed at room temperature except for methanol fixation, which was done on ice. Primary and secondary antibody incubations were 1 h long and were followed by 3-4 washes of 10 min each in PBS+0.2% triton X-100.

Explants were treated with 0.1% saponin in PBS for 40 sec and fixed for 1 h in cold methanol on ice before staining. For LROs (Figures 2A and S2B), we collected stage 16 *Xenopus* embryos, fixed them in 4% PFA for 1 h, washed in PBS and dissected the LROs in MBSH (Modified Barth Solution-H: 88mM NaCl, 1 mM KCl, 2.4 mM $NaHCO_3$, 0.82 mM $MgSO_4$, 0.33 mM $Ca(NO_3)_2$, 0.41 mM $CaCl_2$, 10 mM HEPES (pH 7.6)) as previously described (Schweickert et al., 2007). LROs were then rinsed in PBS+0.2% triton X-100+3% BSA for 1 h and subsequently stained with anti-acetylated tubulin for 1 h, washed, and incubated with an AF488 anti-mouse secondary antibody for 1 h, washed and then incubated for 45 min with Phalloidin (AF647 Phalloidin, Molecular Probes), washed and mounted in coverslips using Prolong Gold antifade reagent (Life Technologies). Hoechst (33342, Life Technologies) was used to stain DNA.

To visualize epidermal cilia (Figures 3A, 3B, S1G and S2D), control, morphant or rescued embryos were collected at stages 28-31 and fixed in 4% PFA for 1-2h. Immunostaining was performed as above with LROs immediately or embryos were dehydrated in 100% ethanol for storage at -20^{o}C and stained later. Embryos were sandwiched between two coverslips with Prolong Gold antifade reagent (Life Technologies) and each side of a single embryo was imaged.

Human RPE cells were treated with 0.1% saponin in PBS for 40 seconds and immediately fixed in cold methanol on ice for 10 minutes. Cells were blocked in PBS, 0.2% triton X-100, 3% BSA for 30 min and then stained sequentially with primary and secondary antibodies.

To localize SNAP-Nup188 (Keppler et al., 2003), HeLa cells were transfected with SNAP-Nup188 using Lipofectamine 2000 (Thermo Fisher). 6 hours after transfection, cells were re-seeded onto glass coverslips. 48 hours after transfection, cells were stained with the cell permeable SNAP substate Oregon Green (New England Biolabs; 1:500) following the manufacturer's instructions prior to fixation.

Conventional fluorescence imaging and analysis

Imaging of whole embryos was performed on a Zeiss Axiovert microscope equipped with Apotome optical interference imaging to obtain optical sections (Figures 3A, 3B, S1G, S2D). Images in Figures 4C, 4D, 4G, 4H, S3A and S3B and S3D were acquired on a Deltavision widefield deconvolution microscope (Applied Precision/GE Healthcare) with a CoolSnap HQ2 CCD camera (Photometrics). The DeltaVision microscope is equipped with an oil Plan Apochromat N 60x/1.42 NA objective (Olympus). Confocal images (Figures 4A and 4B) were obtained using a Leica TCS SP5 microscope equipped with a 100x/1.4 NA oil immersion objective lens (HCX PL APO, Leica Microsystems) and HeNe 633 nm and 488 nm Argon ion lasers, respectively. Confocal images of the LROs (Figures 2 and S2B) were obtained using a Leica TCS SP8 STED 3x microscope equipped with a 20x/0.75 NA and 63x/1.4 NA oil

immersion objectives lens (HCX PL APO, Leica Microsystems), and a SuperK supercontinuum white light laser from NKT Photonics tuned to 488 nm, 594 and/or 633 nm respectively.

All fluorescent micrographs were processed and analyzed using Fiji/ImageJ software (Schindelin et al., 2012). In some cases (images presented in Figures 4C, 4D, 4G, 4H, S3B and S3C), images were first deconvolved using the iterative algorithm in softWoRx (version 5.5; Applied Precision). All quantification in Fiji, however, was performed using unprocessed images. To evaluate levels of Nup93 and Nup188 after siRNA treatment, regions of interest at the nuclear surface (16 μm^2) and at the base of the cilium (encompassing all cilium base signal) were defined at the z-position of maximum intensity. Mean intensity was measured, which was then normalized to the mean intensity of the background (Figures 4E and 4I) in each individual image. In Figure S3B and S3C line profiles were generated using the "plot profile" function. To count cilia in LROs, we used the "count particles" function.

To quantify nuclear:cytoplasmic ratios of NLS-GFP fluorescence in *Xenopus* explants (Figures 3C and 3E and S2G), the mean intensity of an equal area (5 μm^2) in the nucleus and cytoplasm of individual cells was determined. To evaluate NPC density (Figures 3D and 3F), images were made binary and a Gaussian blur filter was applied. To count NPCs, the "find maxima" function was employed. NPC density was assessed by dividing the maxima count over the area in which it was determined.

Further quantification, data plotting and statistical analyses was performed in GraphPad Prism version 6.00, GraphPad Software, La Jolla California USA, www.graphpad.com.

Super-resolution Imaging and analysis

2D FPALM imaging

Immunostained samples were washed twice with freshly prepared dSTORM buffer (Huang et al., 2013) (50 mM Tris pH 8.0, 50 mM NaCl, 10% glucose and 1% β-mercaptoethanol). Immediately before imaging, the oxygen scavengers, glucose oxidase and catalase, were added at a final concentration of 1 kU/mL. Samples were subsequently sealed with parafilm before imaging. Samples immunolabeled for Nup93 and Nup188 (labeled with AF647) and AcTub (labeled with Cy3B) were imaged on a custom built 2D FPALM setup as described previously (Huang et al., 2013; Lin et al., 2015). Samples were illuminated using a 642 nm laser at ~15 kW/cm^2 and 560 nm laser at ~7 kW/cm^2 as readout lasers, respectively. During super-resolution data acquisition, a 405 nm laser was used for fluorophore activation, which was manually controlled to achieve optimal emitter density for single-molecule localization analysis. Emitted fluorescence was collected by a 100x/1.46-NA oil-immersion objective (alpha Plan-Apochromat 100x/1.46 oil, Zeiss) and passed through a multi-band dichroic beamsplitter (FF408/504/581/667/762-Di01-25x36, Semrock) followed by a bandpass filter (FF01-440/521/607/694/809-25, Semrock), and finally a custom beamsplitter (T640SPXR, Chroma). AF 647-emitted light was filtered (ET700/75m) and imaged onto a sCMOS camera (ORCA-Flash 4.0, Hamamatsu) which recorded at 200 FPS using HCImage (Hamamatsu). Cy3B-emitted light was filtered (ET605/70m, Chroma) and collected at 100 FPS. Images were reconstructed as described previously (Huang et al., 2013).

2D FPALM image analysis

To determine the resolution of our system, the localization uncertainty was measured over the course of multiple imaging experiments. These measurements were averaged to obtain the mean localization uncertainty and the standard error in the fitted position of each molecule (σ), which was 12.6 nm and corresponds to a full width at half maximum of ~30 nm.

To calculate the density of the Nup93/Nup188 localizations, we measured the density of local maxima in the reconstructed image that appeared on the nuclear envelope and at the base of the cilia using Fiji/ImageJ software. Specifically, regions of the nuclear envelope and cilia bases were manually selected for processing, images were thresholded and maxima counted

with the “find maxima” tool. In order to compare the size of localization clusters at NPCs and at the bases of cilia, the diameters of clusters were measured using the line profile tool in Fiji/ImageJ software (Schindelin et al., 2012).

W-4PiSMSN (3D) acquisition

For imaging on our custom W-4PiSMSN microscope, sample coverslips were first drained and mounted on a custom sample holder. 50 µL of dSTORM buffer (Huang et al., 2013) (50 mM Tris pH 8.0, 50 mM NaCl, 10% glucose and 1% β-mercaptoethanol) was added to the center of the coverslip and another coverslip was put on top; excess buffer was drained before sealing with a silicone-based sealant (Picodent Twinsil, Picodent, Wipperfürth, Germany). After solidification of the sealant, the samples were transferred to the W-4PiSMSN microscope for imaging.

The W-4PiSMSN microscope is equipped with two opposing 100X 1.4 NA objectives. The system is designed such that the collected fluorescent emission from both objectives are coherently combined to generate an interference pattern of single molecules at the same time (Huang et al., 2016). This allows for about 7-fold higher axial resolution than conventional super-resolution microscopy methods (Baddeley et al., 2011; Huang et al., 2008; Juette et al., 2008; Pavani et al., 2009) and allows generation of 3D images with isotropic resolution in all three dimensions (Huang et al., 2016). The microscope uses excitation light from two lasers emitting at 642 nm (MPB Communications, 2RU-VFL-P-2000-642-B1R) and 560 nm (MPB Communications, 2RU-VFL-2000-560-B1R), and an activation laser at 405 nm (Coherent OBIS 405 LX, 50 mW). Raw W-4PiSMSN data were collected with a sCMOS camera (Hamamatsu, ORCA-Flash 4.0v2) at 100 frames per second (FPS). The entire system is controlled electronically by a custom program written in LabVIEW (National Instruments). The recorded camera frames were subsequently analyzed using custom-designed software written in MatLab (Mathworks) where parts of the algorithms were written through an interface between MatLab, C and CUDA (Nvidia) for massively parallelized computing on a Graphics Processing Unit. The full system design and algorithms are described in detail in Huang et al. (2016).

W-4PiSMSN (3D) image analysis

Nearest neighbor distances: To identify clusters of localizations in 3D point cloud data, images were first de-noised by eliminating isolated points based on Euclidian distance where the local density was calculated from individual single-molecule position estimates. Isolated molecule positions were identified as such when their local density values were lower than a manual threshold (below 20 localizations within a 100 nm (radius) sphere). The de-noised dataset was subsequently analyzed for clusters based on the same distance measurement. We defined a group of single-molecule localizations as a cluster (grouping radius 35 nm) if the number of localizations within the group was above 20. Subsequently, the centers of the clusters were determined by calculating their centroids, and the nearest neighbor distance of a cluster center was calculated based on its minimum Euclidian distance to other centers within a Nup188 structure.

Cylinder fitting: To extract the orientation of the space enclosed by Nup188 for each identified structure, we modeled a cylinder where the location and orientation of the cylinder, described by the cylinder’s central axis ($\boldsymbol{a}$ and $\vec{\boldsymbol{v}}$ represent a point on the axis and the direction of the axis, respectively) and its diameter (r), were determined by regression. We minimized a cost function based on the minimum distance from a single-molecule location ($\boldsymbol{p}$) to the cylinder surface using $d_{min} = \left(\frac{|\overrightarrow{\boldsymbol{pa}}\times\vec{\boldsymbol{v}}|}{|\vec{\boldsymbol{v}}|} - r\right)$ where $\overrightarrow{\boldsymbol{pa}}$ describes a vector from $\boldsymbol{p}$ to $\boldsymbol{a}$. The l_1-norm instead of the l_2-norm of the measured distances was minimized to allow convergence. Both structures in Figure 6

were globally fit with respect to the diameter of the two cylinders. The cylinders were modeled under the assumption of an open end with infinite length. For visualization, however, we manually defined the length as shown in the figures.

In Figures 6 and S6, distances to the cylinder surface (called 'Residue') were measured by calculating the 3D distance of each single-molecule detection from the central axis of the cylinder and then subtracting the cylinder radius. Figure S6 shows the quantification of additional cylinder-modeled structures from W-4PiSMSN not shown in Figure 6.

To determine the uncertainty of the cylinder radius estimates, we implemented a bootstrapping method using 100 resamples with replacement (Efron and Tibshirani, 1993). The radii of the cylinder models were obtained by either fitting simultaneously both daughter and mother centrioles with two cylinders (global fit) or a single centriole (single fit). In global fit, to facilitate the bootstrapping resampling, we first resampled independently from the pools of both centrioles making the number of localization events equal on both centrioles and then proceeded with bootstrapping. The estimated mean radii and their uncertainties determined from the bootstrapping method are listed in Table S1.

Cluster size measurements: In Figure S5, nearest-neighbor distances were calculated from regions of interest (ROIs) selected outside the basal body and around a basal body, respectively. The number of localization events per cluster, called "detections per cluster", was calculated based on a cluster grouping radius of 35 nm (see '*Nearest neighbor distances*' section above).

In Figure S4B-D, the number of localizations listed for representative clusters in the figures was quantified from the single-molecule localization data itself by counting the number of localizations in each identified cluster. This step was done for all clusters from the 3 ROIs.

Stimulated emission depletion (STED) microscopy imaging

Two-color STED imaging of samples immunolabeled for Nup188 (ATTO647N) and γ-tubulin (ATTO594) or acetylated tubulin (ATTO594) were performed on a Leica SP8 STED microscope equipped with a white light excitation laser and a 775-nm pulsed depletion laser. Four images were taken for each field of view; one confocal and one STED for each of the two colors.

STED image analysis

Cluster intensity measurements: In Figure S4E, noted intensity values (a.u.) are average counts per pixel in the selected square regions (white boxes).

Table S1 – Mean radii and uncertainties of fitted cylinders

W-4PiSMSN Structures	Radius (r, nm)	∆r (nm)	Data Presented	Fit type
Struct 1	218	6.7	Movie S2, Figure 6	Global
Struct 2	218	6.7	Movie S2, Figure 6	Global
Struct 3	174	0.9	Movie S3, Figure S6	Single
Struct 4	167	2.6	Movie S3, Figure S6	Single
Struct 5	179	1.2	Movie S3, Figure S6	Single
Struct 6	173	1.3	Movie S3, Figure S6	Single
Struct 7	171	0.7	Movie S3, Figure S6	Single

Table S1 – (Related to Figure 6 and Experimental procedures): Mean radii and uncertainties of fitted cylinders

Using a bootstrapping method, we calculated the mean radii of fitted cylinders and the uncertainty (Δr) of this measurement to the Nup188 structure as determined by W-4PiSMSN data. In the case of Struct 1 and 2, we fitted two cylinders simultaneously to the overall structures (global fit) while in the remaining structures, we fitted a single cylinder to the data (single fit).

Supplementary References

Baddeley, D., Cannell, M.B., and Soeller, C. (2011). Three-dimensional sub-100 nm super-resolution imaging of biological samples using a phase ramp in the objective pupil. Nano Research *4*, 589-598.

Boskovski, M.T., Yuan, S., Pedersen, N.B., Goth, C.K., Makova, S., Clausen, H., Brueckner, M., and Khokha, M.K. (2013). The heterotaxy gene GALNT11 glycosylates Notch to orchestrate cilia type and laterality. Nature *504*, 456-459.

del Viso, F., and Khokha, M. (2012). Generating diploid embryos from *Xenopus tropicalis*. Methods in molecular biology *917*, 33-41.

Efron, B., and Tibshirani, R.J. (1993). An Introduction to the Bootstrap (New York: Chapman and Hall).

Franz, C., Walczak, R., Yavuz, S., Santarella, R., Gentzel, M., Askjaer, P., Galy, V., Hetzer, M., Mattaj, I.W., and Antonin, W. (2007). MEL-28/ELYS is required for the recruitment of nucleoporins to chromatin and postmitotic nuclear pore complex assembly. EMBO reports *8*, 165-172.

Huang, B., Jones, S.A., Brandenburg, B., and Zhuang, X. (2008). Whole-cell 3D STORM reveals interactions between cellular structures with nanometer-scale resolution. Nature methods *5*, 1047-1052.

Huang, F., Hartwich, T.M., Rivera-Molina, F.E., Lin, Y., Duim, W.C., Long, J.J., Uchil, P.D., Myers, J.R., Baird, M.A., Mothes, W.*, et al.* (2013). Video-rate nanoscopy using sCMOS camera-specific single-molecule localization algorithms. Nature methods *10*, 653-658.

Huang, F., Sirinakis, G., Allgeyer, E.S., Schroeder, L.K., Duim, W.C., Kromann, E.B., Phan, T., Rivera-Molina, F.E., Myers, J.R., Irnov, I.*, et al.* (2016). Ultra-High Resolution 3D Imaging of Whole Cells. Cell. http://dx.doi.org/10.1016/ j.cell.2016.06.016

Juette, M.F., Gould, T.J., Lessard, M.D., Mlodzianoski, M.J., Nagpure, B.S., Bennett, B.T., Hess, S.T., and Bewersdorf, J. (2008). Three-dimensional sub-100 nm resolution fluorescence microscopy of thick samples. Nature methods *5*, 527-529.

Keppler, A., Gendreizig, S., Gronemeyer, T., Pick, H., Vogel, H., and Johnsson, K. (2003). A general method for the covalent labeling of fusion proteins with small molecules in vivo. Nat Biotechnol *21*, 86-89.

Khokha, M.K., Chung, C., Bustamante, E.L., Gaw, L.W., Trott, K.A., Yeh, J., Lim, N., Lin, J.C., Taverner, N., Amaya, E.*, et al.* (2002). Techniques and probes for the study of *Xenopus tropicalis* development. Dev Dyn *225*, 499-510.

Kwan, K.M., Fujimoto, E., Grabher, C., Mangum, B.D., Hardy, M.E., Campbell, D.S., Parant, J.M., Yost, H.J., Kanki, J.P., and Chien, C.B. (2007). The Tol2kit: a multisite gateway-based construction kit for Tol2 transposon transgenesis constructs. Dev Dyn *236*, 3088-3099.

Lin, Y., Long, J.J., Huang, F., Duim, W.C., Kirschbaum, S., Zhang, Y., Schroeder, L.K., Rebane, A.A., Velasco, M.G., Virrueta, A.*, et al.* (2015). Quantifying and optimizing single-molecule switching nanoscopy at high speeds. PloS one *10*, e0128135.

Mishra, R.K., Chakraborty, P., Arnaoutov, A., Fontoura, B.M., and Dasso, M. (2010). The Nup107-160 complex and gamma-TuRC regulate microtubule polymerization at kinetochores. Nature cell biology *12*, 164-169.

Nieuwkoop, P.D., and Faber, J. (1994). Normal table of *Xenopus laevis* (Daudin) : a systematical and chronological survey of the development from the fertilized egg till the end of metamorphosis. (Garland Pub.).

Pavani, S.R., Thompson, M.A., Biteen, J.S., Lord, S.J., Liu, N., Twieg, R.J., Piestun, R., and Moerner, W.E. (2009). Three-dimensional, single-molecule fluorescence imaging beyond the diffraction limit by using a double-helix point spread function. Proc Natl Acad Sci U S A *106*, 2995-2999.

Schindelin, J., Arganda-Carreras, I., Frise, E., Kaynig, V., Longair, M., Pietzsch, T., Preibisch, S., Rueden, C., Saalfeld, S., Schmid, B.*, et al.* (2012). Fiji: an open-source platform for biological-image analysis. Nature methods *9*, 676-682.

Schweickert, A., Campione, M., Steinbeisser, H., and Blum, M. (2000). Pitx2 isoforms: involvement of *Pitx2c* but not *Pitx2a* or *Pitx2b* in vertebrate left-right asymmetry. Mechanisms of development *90*, 41-51.

Schweickert, A., Vick, P., Getwan, M., Weber, T., Schneider, I., Eberhardt, M., Beyer, T., Pachur, A., and Blum, M. (2010). The nodal inhibitor *Coco* is a critical target of leftward flow in *Xenopus*. Current biology : CB *20*, 738-743.

Schweickert, A., Weber, T., Beyer, T., Vick, P., Bogusch, S., Feistel, K., and Blum, M. (2007). Cilia-driven leftward flow determines laterality in Xenopus. Curr Biol *17*, 60-66.

Theerthagiri, G., Eisenhardt, N., Schwarz, H., and Antonin, W. (2010). The nucleoporin Nup188 controls passage of membrane proteins across the nuclear pore complex. The Journal of cell biology *189*, 1129-1142.

Werner, M.E., and Mitchell, B.J. (2013). Using *Xenopus* skin to study cilia development and function. Methods in enzymology *525*, 191-217.